JCI insight

Molnupiravir inhibits SARS-CoV-2 variants including Omicron in the hamster model

Kyle Rosenke, … , Michael A. Jarvis, Heinz Feldmann

JCI Insight. 2022. https://doi.org/10.1172/jci.insight.160108.

Research In-Press Preview **COVID-19** **Virology**

The recent emergence of the SARS-CoV-2 Omicron variant of concern (VOC) containing a heavily mutated spike protein capable of escaping preexisting immunity identifies a continued need for interventional measures. Molnupiravir (MK-4482), an orally administered nucleoside analog, has demonstrated efficacy against earlier SARS-CoV-2 lineages and was recently approved for SARS-CoV-2 infections in high-risk adults. Here we assessed the efficacy of MK-4482 against the earlier Alpha, Beta and Delta VOCs and Omicron in the hamster COVID-19 model. Omicron replication and associated lung disease in vehicle treated hamsters was reduced compared to the earlier VOCs. MK-4482 treatment inhibited virus replication in the lungs of Alpha, Beta and Delta VOC infected hamsters. Importantly, MK-4482 profoundly inhibited virus replication in the upper and lower respiratory tract of hamsters infected with the Omicron VOC. Consistent with its mutagenic mechanism, MK-4482 treatment had a more pronounced inhibitory effect on infectious titers compared to viral RNA genome load. Histopathologic analysis showed that MK-4482 treatment caused a concomitant reduction in the level of lung disease and viral antigen load in infected hamsters across all VOCs examined. Together, our data indicate the potential of MK-4482 as an effective antiviral against known SARS-CoV-2 VOCs, especially Omicron, and likely future SARS-CoV-2 variants.

Title: Molnupiravir inhibits SARS-CoV-2 variants including Omicron in the hamster model

Authors: Kyle Rosenke[1], Atsushi Okumura[1], Matthew C. Lewis[1], Friederike Feldmann[2], Kimberly Meade-White[1], W. Forrest Bohler[1], Amanda Griffin[1], Rebecca Rosenke[2], Carl Shaia[2], Michael A. Jarvis[1,3,4]*, Heinz Feldmann[1]*

Affiliations: [1]Laboratory of Virology, [2]Rocky Mountain Veterinary Branch, National Institute of Allergy and Infectious Diseases, National Institutes of Health; Hamilton, MT, USA; [3]School of Biomedical Sciences, University of Plymouth; Plymouth, Devon, UK; [4]The Vaccine Group Ltd; Plymouth, Devon, UK.

***Corresponding authors:** Heinz Feldmann, Rocky Mountain Laboratories, 903 S 4th Street, Hamilton, MT, US-59840; Tel: (406)-375-7410; Email: feldmannh@niaid.nih.gov; Michael A. Jarvis, University of Plymouth, School of Biomedical Sciences, Derriford Research Facility, Plymouth, Devon, UK, PL6 8BU; Tel: +44 (0)1752-437444; Email: michael.jarvis@plymouth.ac.uk

One Sentence Summary: MK-4482 inhibits replication of multiple SARS-CoV-2 variants of concern, including Omicron, in the Syrian hamster COVID-19 model

Conflict of Interest Statement: The authors have declared that no conflict of interest exists.

ABSTRACT

The recent emergence of the SARS-CoV-2 Omicron variant of concern (VOC) containing a heavily mutated spike protein capable of escaping preexisting immunity identifies a continued need for interventional measures. Molnupiravir (MK-4482), an orally administered nucleoside analog, has demonstrated efficacy against earlier SARS-CoV-2 lineages and was recently approved for SARS-CoV-2 infections in high-risk adults. Here we assessed the efficacy of MK-4482 against the earlier Alpha, Beta and Delta VOCs and Omicron in the hamster COVID-19 model. Omicron replication and associated lung disease in vehicle treated hamsters was reduced compared to the earlier VOCs. MK-4482 treatment inhibited virus replication in the lungs of Alpha, Beta and Delta VOC infected hamsters. Importantly, MK-4482 profoundly inhibited virus replication in the upper and lower respiratory tract of hamsters infected with the Omicron VOC. Consistent with its mutagenic mechanism, MK-4482 treatment had a more pronounced inhibitory effect on infectious titers compared to viral RNA genome load. Histopathologic analysis showed that MK-4482 treatment caused a concomitant reduction in the level of lung disease and viral antigen load in infected hamsters across all VOCs examined. Together, our data indicate the potential of MK-4482 as an effective antiviral against known SARS-CoV-2 VOCs, especially Omicron, and likely future SARS-CoV-2 variants.

INTRODUCTION

Now in its third year, the coronavirus disease 2019 (COVID-19) pandemic has become characterized by the serial emergence of severe acute respiratory syndrome coronavirus 2

(SARS-CoV-2) variants of concern (VOCs) that rapidly and globally replace earlier, previously predominant strains. In November 2021, Omicron (B.1.1.529) emerged to rapidly replace Delta (B.1.617.2), the predominant VOC at the time (1). Omicron has shown reduced pathogenicity (2) but enhanced transmissibility primarily associated with an increased ability to evade protective immunity associated with infection by earlier VOCs or through vaccination (3, 4). The emergence of such VOCs with immune evasive ability poses a continuous and considerable threat to global control strategies based on present spike-based vaccines, as well as monoclonal antibody-based therapeutics for treatment of more severe COVID-19.

Molnupiravir (MK-4482) is an orally available antiviral nucleoside analogue that targets SARS-CoV-2 polymerase fidelity rather than the spike protein (5). It has been authorized for emergency use against SARS-CoV-2 in high-risk adults (6, 7). Studies from early in the pandemic showed the ability of MK-4482 to suppress acute virus replication and associated disease in the Syrian hamster COVID-19 model (8) and transmission in ferrets (9). Both of these early studies were performed before VOC emergence became the norm and showed effect against the original Washington SARS-CoV-2 variant which was still prevalent at this time. Later in the pandemic, efficacy in hamsters was shown against Alpha and Beta VOCs, which were emerging at the time (10). Results from recent in vitro studies suggest that molnupiravir retains activity against multiple VOCs including the more pathologic Delta and transmissible Omicron variants (11). However, experience with therapeutics targeting SARS-CoV-2 (12), as well as other emerging viruses (13) have shown a frequent disconnect between efficacy observed in vitro compared to therapeutic in vivo effect.

In the present study we investigate the ability of MK-4482 to inhibit several SARS-CoV-2 VOCs in the Syrian hamster COVID-19 model. MK-4482 reduced viral RNA loads and significantly

reduced infectious virus in the lungs for Omicron as well as Alpha, Beta and Delta VOCs. Notably, MK-4482 also significantly reduced infectious virus in oral swabs and the upper and lower respiratory tracts in hamsters infected with a high dose of Omicron. Our study demonstrates efficacy of MK-4482 against multiple divergent VOCs including Omicron and is likely an effective antiviral against future emerging SARS-CoV-2 variants.

RESULTS

Syrian hamsters were randomly divided into vehicle- or MK-4482-treatment groups, and infected intranasally with 10^3 $TCID_{50}$ as previously established (14) to test in vivo efficacy of MK-4482 against the SARS-CoV-2 Alpha, Beta, Delta and Omicron VOCs. Treatment using 250mg/kg MK-4482, administered by oral gavage, was initiated 12h after infection. Treatment was continued every 12h for the established total daily dose of 500mg/kg (8). Hamsters were monitored daily for clinical signs and oral swabs were collected 2 and 4 days post-infection (dpi). At 4 dpi hamsters were euthanized and tissues collected for viral RNA load and infectious titer determination (Figure 1A).

Hamsters in vehicle and MK-4482 treatment groups remained largely asymptomatic with noticeable but not significant weight loss (3-4%) in vehicle treated animals over the 4-day study period (Figure 1B). Quantitative RT-PCR (qRT-PCR) targeting subgenomic viral E gene RNA (sgE) in oral swabs and lung tissue was used to quantify replication in the upper and lower respiratory tract, respectively (15). sgE loads in oral swabs from vehicle treated animals on 2 and 4 dpi ranged from 5 to 8 log_{10} copies/mL confirming infection by all VOCs with the exception of a single Omicron animal (Figure 1C). MK-4482 treatment resulted in lower replication in oral swabs for all VOCs except Delta, a result that was only statistically significant for Omicron at 2

dpi (Figure 1C). sgE loads in lung tissue ranged from 7 to 10 log_{10} copies/g for Alpha, Beta and Delta in vehicle treated groups, but was notably lower (0-7 log_{10} copies/g) for Omicron (Figure 1D). MK-4482 treatment resulted in a reduction in sgE lung loads for all VOCs and was below the limit of detection for Omicron, a result that was statistically significant (Figure 1D). Similarly, infectious virus titers in lung tissue ranged from 6-11 log_{10} $TCID_{50}$/g for Alpha, Beta and Delta vehicle treated groups that was significantly lower for Omicron (0 to 6 log_{10} $TCID_{50}$/g) (Figure 1E). Infectious titers were substantially more reduced by MK-4482 than sgE loads. This was observed for all VOCs, with no infectious virus detected in lung tissue from any Omicron infected hamster (Figure 1E).

Histopathologic analysis of lung tissues revealed minimal to moderate broncho-interstitial pneumonia for vehicle treated Alpha, Beta and Delta VOC infected hamsters (Figure 2). Omicron infected animals showed only mild lesions reflecting reduced virus replication of this VOC in the lower respiratory tract (16) (Figure 2). In general lesions were as previously described (14). They consisted of bronchiolar and alveolar inflammation most prominent around terminal bronchioles with neutrophils, macrophages, necrotic debris, fibrin and edema in associated alveolar spaces as well as variable amounts of septal inflammation and thickening (Figure 3). Other features included single and small clusters of necrotic respiratory epithelium in large and medium caliber bronchioles and vasculitis in locally associated blood vessels (Figure 3). Lesions were reduced in all MK-4482 treated hamsters as noticeably and best shown on the lung hematoxylin and eosin (H&E) overview stains (Figure 2) but also in the higher magnified H&E detailed stains (Figure 3). Immunohistochemical labeling of affected and non-affected bronchioles and alveoli was common throughout, but especially at the margins of regions of pneumonia for vehicle treated hamsters infected with the Alpha, Beta and Delta VOCs (Figure 2;

Figure 3). Labeling was only infrequently found with hamsters infected with the Omicron VOC (Figure 2; Figure 3). Immunoreactivity was consistently less frequent in MK-4482 treated hamsters for each group with basically no immunoreactivity in the treated Omicron infected hamsters (Figure 2; Figure 3)

We repeated the MK-4482 treatment study with a higher Omicron challenge dose (10^4 $TCID_{50}$) to account for the decreased replication of the Omicron VOC in lung tissue (16, 17). The study design remained the same as described above (Figure 1A), but trachea tissue was collected at 4 dpi as an additional target tissue. The higher Omicron challenge dose did not increase clinical disease severity and weight loss remained similar to animals challenged with the lower 10^3 $TCID_{50}$ dose (Figure 1B). At 2 and 4 dpi, sgE loads of oral swabs from vehicle treated animals ranged from 5 to 7 log_{10} copies/mL, which were lower in MK-4482 treated animals (<1 log_{10} copies/mL), a difference that was not statistically significant (Figure 4A). Infectious virus in oral swabs from vehicle treated animals ranged from 4 to 7 log_{10} $TCID_{50}$/mL (Figure 4B), which was significantly reduced by several log_{10} following MK-4482 treatment (Figure 4B). sgE loads and infectious titers were also determined in trachea and lung tissues at 4 dpi. In contrast to trachea, approximately half the animals in the vehicle treated group lacked detectable virus in the lung (by $TCID_{50}$) consistent with lower replication of Omicron in this tissue in general (16). Remarkably, MK-4482 treatment reduced sgE loads and infectious virus to below the limit of detection in lung tissue of all animals, corresponding to an average reduction by >4 log_{10} (Figure 4C) and >2 log_{10} (Figure 4D), respectively. Interestingly, sgE loads were several log_{10} higher in trachea (9 to 11 log_{10} copies/g) compared to lung tissue of vehicle treated hamsters (Figure 4C). sgE loads were less than a log_{10} lower in trachea tissue from MK-4482 treated animals (Figure 4C). However, infectious virus in trachea tissue dropped precipitously from a median of 5 log_{10}

$TCID_{50}$/g in vehicle treated animals to below the limit of detection in MK-4482 animals (Figure 4D). Histopathologic analysis of the lungs confirmed the findings on viral loads and infectious titers in lung tissue showing reduced lesions (Figure 4E,F) and no viral antigen (Figure 4G,H) in the MK-4482 treated Omicron infected hamsters.

DISCUSSION

Since SARS-CoV-2 emerged in late 2019, there have been at least 13 variants of interest (VOI) or VOCs circulating throughout the world (18). As each variant is likely to become more adapted at spread and avoiding preexisting immunity developed by previous infection or vaccination, refining existing and developing new treatment options becomes critically important for our response to the SARS-CoV-2 pandemic. In this study we evaluated the efficacy of MK-4482 against several SARS-CoV-2 VOCs in the Syrian hamster model. MK-4482 was efficacious against all VOCs with significant reduction of virus replication in the lower respiratory tract. This was particularly evident for the Omicron VOC with absence of any infectious virus in trachea and lung samples. Thus, molnupiravir remains potent against SARS-CoV-2 variants including Omicron, likely positively affecting COVID-19 patient outcome.

Important for transmission, a key driver of any epidemic and pandemic, is the impact of an antiviral intervention on virus shedding. In contrast to SARS-CoV-2 replication in the lower respiratory tract, MK-4482 treatment only slightly decreased replication and shedding from the upper respiratory tract for the Alpha, Beta and Delta VOCs. Interestingly, MK-4482 treatment significantly reduced replication and shedding of Omicron, indicating potent efficacy against the VOC driving the current SARS-CoV-2 pandemic. This is a somewhat surprising but rather

encouraging result with the potential of positively influencing the course of the current pandemic wave.

The antiviral activity of MK-4482 is not affected by mutations in the spike protein and remains active against all variants of SARS-CoV-2. Thus, MK-4482 remains a potent alternative to monoclonal antibody treatment which is rather vulnerable to mutations in the spike protein (11). Although Omicron already has mutations in the viral polymerase protein (19), the target of MK-4482 antiviral action, the drug remains effective against this VOC with significant reduction of viral replication in the upper and lower respiratory tract. It remains to be seen whether future variants that may develop under more widespread clinical use of molnupiravir will acquire further mutations in the polymerase resulting in reduced drug activity or even loss of drug efficacy. Nevertheless, serial in vitro passage studies of several RNA viruses (20, 21) as well as related coronaviruses (22) under suboptimal levels of the active metabolite of MK-4482 indicate a high genetic barrier of the drug to the acquisition of viral resistance. Selective and targeted clinical use of the drug as well as the consideration of combination therapy with synergistic antivirals or other therapeutic approaches (23) may also help to reduce the development of such drug resistance.

We found a marked discrepancy between viral sgRNA loads and infectious titers for all MK-4482 treated VOCs. Given the mechanism of action of MK-4482 (5) this may not be surprising as mutated, replication incompetent viral RNA will still be detected by qRT-PCR analysis but not by infectivity assays. This observation emphasizes the need to consider the specific method of analysis being used to assess antiviral activity, as viral sgRNA loads are often used as the single measure for SARS-CoV-2 replication. Our results strongly suggest that infectious titers are critical for a complete investigation and required to determine the efficacy of antiviral drugs

and likely also vaccines. Histopathology serves as an important confirmation for virus replication in target tissues and provides valuable pathologic images.

Our study has limitations. The hamster model does not accurately represent COVID-19 disease for all human age- and comorbidity-associated subpopulations as the animals only develop mild-to-moderate disease (14, 24, 25), but this is a drawback of most current COVID-19 animal models (26). The more recently identified dwarf hamster model is associated with higher disease severity, but the extremely acute disease progression with animals reaching clinical endpoints within as quickly as 3 dpi (27) does not parallel the more prolonged course of severe disease in humans (28). In all models, the current intranasal delivery of the challenge virus, whilst mimicking the most biologically relevant route of infection in humans, may interfere with readout parameters for the upper respiratory tract negatively impacting analysis of virus replication and shedding. Future transmission studies need to confirm the impact of MK-4482 on virus shedding and ultimately transmission to naïve animals. A study awaiting peer-review has shown an inhibitory effect of MK-4482 on shedding and transmission in the upper respiratory disease ferret model (29), which is encouraging. However, studies investigating the direct transmission from infected to naïve animals are more difficult to perform in the hamster (30) and should be targeted for future experiments. The greatest limitation in the current situation is the incomplete experience with molnupiravir in clinical studies against the Omicron VOC. Further studies are underway, and results are expected in the near future. Nevertheless, in vitro studies (11), preclinical data from animal models such as our study and others (26), and previous clinical trials against earlier SARS-CoV-2 VOCs (6) strongly support the use of molnupiravir for mild-to-moderate COVID cases of Omicron in high-risk adults as well as possibly for postexposure prophylaxis.

In conclusion, our data demonstrate potent efficacy of MK-4482 against the dominant Omicron VOC in a key well-established in vivo COVID-19 disease model. We also demonstrate efficacy of MK-4482 against earlier globally distributed VOCs identifying molnupiravir as an important broad-acting antiviral intervention for existing and likely future VOCs. The potent efficacy and favorable route of oral administration support further clinical development and broader use of molnupiravir as a key treatment option for SARS-CoV-2 infections in humans.

METHODS

Biosafety and ethics. SARS-CoV-2 work was approved by the Institutional Biosafety Committee (IBC) and performed in high biocontainment at Rocky Mountain Laboratories (RML), NIAID, NIH. IBC-approved Standard Operating Protocols were followed for sample removal from biocontainment. Institutional Animal Care and Use Committee approved all animal work which was performed by certified staff in an Association for Assessment and Accreditation of Laboratory Animal Care International accredited facility. The institution's guidelines for animal use, the guidelines and basic principles in the NIH Guide for the Care and Use of Laboratory Animals, the Animal Welfare Act, United States Department of Agriculture and the United States Public Health Service Policy on Humane Care and Use of Laboratory Animals were followed. Syrian hamsters were group housed in HEPA-filtered cage systems enriched with nesting material and were provided with commercial chow and water ad libitum. Animals were monitored at least twice daily.

Syrian hamster study design. Male and female 8–10-week-old Syrian Golden hamsters (Envigo, Livermore, CA, USA) were divided into vehicle (N=15 for Omicron infected, N=11

Alpha, Beta, Delta infected) or treatment (N=10 for Alpha, Beta, Delta, Omicron infected; N=9 for the Omicron high dose infected) groups prior to infection and treatments with MK-4482 (MedChemExpress, Monmouth Junction, NJ, USA). MK-4482 was dissolved in DMSO and then resuspended in sterile saline for delivery at 250mg/kg. Hamsters were treated 12 hours following infection, and treatment was continued every 12 hours until the completion of the study 84 hours post-infection (day 4). Vehicle control animals received the same dosing schedule and volume as VOC infection groups. All groups were infected intranasally with 10^3 or 10^4 $TCID_{50}$ (high dose to account for reduced replication of Omicron (17) of SARS-CoV-2 via (25 µL/nare). Intranasal inoculations were performed as previously described (14). In brief, hamsters were anesthetized with vaporized isoflurane and 25 µL of inoculum was dropped into each naris by pipette for a total infection volume of 50 µL. Animal weights were collected once daily, and animals were monitored twice daily for disease signs and progression. All procedures were performed on anesthetized animals. Oral swabs were collected on days 2 and 4 post-infection. Animals were euthanized on day 4 post-infection and trachea and lung tissues were collected at necropsy for analysis.

Virus and cells. The SARS-CoV-2_2hCOV_19_England_204820464_2020 isolate (B.1.1.7; Alpha) was provided by BEI Resources (Manassas, VA, USA). The stock was sequence confirmed and had amino acid changes at ORF1AB (D3725G: 13%) and ORF1AB (L3826F: 18%) when aligned to the GISAID sequence (GISAID # EPI_ISL_683466). SARS-CoV-2 isolate nCoV-hCoV-19/USA/MD-HP01542/2021 (B.1.351, Beta) was provided by Andy Pekosz (Johns Hopkins University, Baltimore, MD, USA). The virus stock was sequence confirmed and found to have amino acid changes at NSP5 (P252L: 17%) and NSP6 (L257F: 57%) when aligned to the GISAID sequence (GISAID # EPI_ISL_890360). SARS-CoV-2 variant hCoV-

19/USA/KY-CDC-2-4242084/2021 (B.1.617.2, Delta) was obtained with contributions from B. Zhou, N. Thornburg and S. Tong (Centers for Disease Control and Prevention, Atlanta, GA, USA). SARS-CoV-2 variant hCoV-19/USA/GA-EHC-2811C/2021 (B.1.1.529, Omicron, EPI_ISL_7171744) was obtained from Mehul Suthar (Emory University, Atlanta, GA, USA). Virus stocks for use in the in vivo studies were produced in VeroE6 cells. All viral stocks were sequenced via Illumina-based deep sequencing to confirm identity and exclude any contaminants. Virus propagation was performed in DMEM (Sigma, St. Louis, MO, USA) supplemented with 2% fetal bovine serum (Gibco Waltham, MA, USA), 1 mM L-glutamine (Gibco, Waltham, MA, USA), 50 U/ml penicillin and 50 µg/ml streptomycin (Gibco, Waltham, MA, USA). Vero E6 cells, kindly provided by R. Baric, University of North Carolina, were maintained in DMEM (Sigma, St. Louis, MO, USA) supplemented with 10% fetal calf serum, 1 mM L-glutamine, 50 U/mL penicillin and 50 µg/mL streptomycin.

Viral genome detection. qPCR was performed on RNA extracted from swabs or tissues (30 mg or less) using QiaAmp Viral RNA kit (Qiagen, Hilden, Germany). A one-step real-time RT-PCR assay was used to amplify a portion of the E gene to detect subgenomic RNA (15). Dilutions of RNA standards counted by droplet digital PCR were run in parallel and used to calculate viral RNA genome copies. The Rotor-Gene probe kit (Qiagen, Hilden, Germany) was used to run the PCRs according to the instructions of the manufacturer.

Virus titration assay. Virus end-point titrations were performed in Vero E6 cells. Briefly, tissue was homogenized in 1ml DMEM using a TissueLyzer (Qiagen, Hilden, Germany) and clarified by low-speed centrifugation. Cells were inoculated with 10-fold serial dilutions of homogenized lung samples or oral swabs in 100 µl DMEM (Sigma, St. Louis, MO, USA) supplemented with 2% fetal bovine serum, 1 mM L-glutamine, 50 U/ml penicillin and 50 µg/ml streptomycin. Cells

were incubated for six days and then scored for cytopathogenic effects (CPE) and $TCID_{50}$ was calculated via the Reed-Muench formula.

Histopathology: Tissues were embedded in Pureaffin paraffin polymer (Cancer Diagnostics, Durham, NC, USA) and sectioned at 5 µm for hematoxylin and eosin (H&E) staining. For immunohistochemistry (IHC), tissues were processed using the Discovery Ultra automated stainer (Ventana Medical Systems, Oro Valley, AZ, USA) with a ChromoMap DAB kit (Roche Tissue Diagnostics cat#760-159, Basel, Switzerland). Specific immunoreactivity was detected using GenScript (Piscataway, NJ, USA) SARS-CoV-2-specific antiserum (U864YFA140-4/CB2093 NP-1) at a 1:1000 dilution. The secondary antibody was an anti-rabbit IgG polymer (cat# MP-6401) from Vector Laboratories ImPress VR (Vernon Hills, IL, USA).

Statistical analyses. Statistical analysis was performed in Prism 9. The Students T-test was a two-tailed with the p-value set to 0.05 for significance ($P<0.05$). The difference in weight, viral load and infectious titers between study arms was assessed by ordinary one-way ANOVA (P-value was set to 0.05).

Study approval. The Institutional Animal Care and Use Committee approved all animal work under protocol 2020-044-E.

AUTHOR CONTRIBUTIONS

K. Rosenke, M.A. Jarvis and H. Feldmann contributed to the design, execution and data analysis, and writing of the manuscript.

A. Okumura, M.C. Lewis, F. Feldmann, K. Meade-White, W.F. Bohler and A. Griffin contributed experimental support and data analysis.

R. Rosenke and C. Shaia contributed to the pathological analysis.

H. Feldmann and M.A. Jarvis secured funding for the study.

ACKNOWLEDGMENTS

The authors thank staff members of the Laboratory of Virology and the Genomics Unit of the Research Technology Branch (both National Institutes of Allergy and Infectious Diseases (NIAID, National Institutes of Health (NIH), Hamilton, MT, USA) for their efforts in providing workable SARS-CoV-2 stocks. The authors also wish to thank the Rocky Mountain Veterinary Branch (NIAID, NIH, Hamilton, MT, USA) for animal care and husbandry. The authors are thankful to Anita Mora (Visual and Medical Arts Unit, NIAID, NIH, Hamilton, MT, USA) for help with graphical design. Isolate SARS-CoV-2_2hCOV_19_England_204820464_2020 isolate (B.1.1.7; Alpha) was obtained through BEI Resources (Bassam Hallis, Sujatha Rashid; Manassas, VA, USA), NIAID (Ranjan Mukul, Kimberly Stemple) and the NIH (Bethesda, MD, USA). Isolate hCoV-19/USA/MD-HP01542/2021 was obtained from Andrew Pekosz, John Hopkins Bloomberg School of Public Health (Baltimore, MD, USA). Isolate hCoV-19/USA/GA-EHC-2811C/2021 was obtained from Mehul Suthar, University Emory School of Medicine (Atlanta, GA, USA). The following reagent was deposited by the Centers for Disease Control and Prevention (Atlanta, GA, USA) and obtained through BEI Resources (Manassas, VA, USA), NIAID, NIH (Bethesda, MD, USA): hCoV-19/USA/KY-CDC-2-4242084/2021. Vero E6 cells were obtained from Dr. Ralph Baric at the University of North Carolina (Chapel Hill, NC, USA).

The work was mainly funded by the Intramural Research Program of NIAID, NIH (Bethesda, MD, USA) and partially through the University of Plymouth (Plymouth, UK).

COMPETING INTERESTS

MAJ is employed, in part, by the Vaccine Group Ltd. All authors declare that they have no competing interests.

DATA AND MATERIALS AVAILABILITY

All data is presented here.

DISCLAIMER

The opinions, conclusions and recommendations in this report are those of the authors and do not necessarily represent the official positions of the National Institute of Allergy and Infectious Diseases (NIAID) at the National Institutes of Health (NIH), The Vaccine Group Ltd or the University of Plymouth.

REFERENCES AND NOTES

1. Karim SSA, and Karim QA. Omicron SARS-CoV-2 variant: a new chapter in the COVID-19 pandemic. *Lancet.* 2021;398(10317):2126-8.

2. European Medicines Agency. Preliminary data indicate COVID-19 vaccines remain effective against severe disease and hospitalisation caused by the Omicron variant. 2022. [Accessed 11Apr22].
3. Cao Y, Wang J, Jian F, Xiao T, Song W, Yisimayi A, et al. Omicron escapes the majority of existing SARS-CoV-2 neutralizing antibodies. *Nature.* 2022;602(7898):657-663.
4. Lyngse FP, Mortensen LH, Denwood MJ, Christiansen LE, Moller CH, Skov RL, et al. SARS-CoV-2 Omicron VOC Transmission in Danish Households. *medRxiv.* 2021.
5. Kabinger F, Stiller C, Schmitzova J, Dienemann C, Kokic G, Hillen HS, et al. Mechanism of molnupiravir-induced SARS-CoV-2 mutagenesis. *Nat Struct Mol Biol.* 2021;28(9):740-6.
6. Jayk Bernal A, Gomes da Silva MM, Musungaie DB, Kovalchuk E, Gonzalez A, Delos Reyes V, et al. Molnupiravir for Oral Treatment of Covid-19 in Nonhospitalized Patients. *N Engl J Med.* 2022;386(6):509-20.
7. FDA. Emergency Use Authorization 108: Letter in response to Merck request that the FDA issue an EUA for the emergency use of molnupiravir for the treatment of mild-to-moderate COVID-19 in certain adults who are at high-risk for progression to severe COVID-19. 2022. [Accessed 11Apr22].
8. Rosenke K, Hansen F, Schwarz B, Feldmann F, Haddock E, Rosenke R, et al. Orally delivered MK-4482 inhibits SARS-CoV-2 replication in the Syrian hamster model. *Nat Commun.* 2021;12(1):2295.
9. Cox RM, Wolf JD, and Plemper RK. Therapeutically administered ribonucleoside analogue MK-4482/EIDD-2801 blocks SARS-CoV-2 transmission in ferrets. *Nat Microbiol.* 2021;6(1):11-8.

10. Abdelnabi R, Foo CS, De Jonghe S, Maes P, Weynand B, and Neyts J. Molnupiravir Inhibits Replication of the Emerging SARS-CoV-2 Variants of Concern in a Hamster Infection Model. *J Infect Dis.* 2021;224(5):749-53.

11. Takashita E, Kinoshita N, Yamayoshi S, Sakai-Tagawa Y, Fujisaki S, Ito M, et al. Efficacy of Antibodies and Antiviral Drugs against Covid-19 Omicron Variant. *N Engl J Med.* 2022;386(10):995-998.

12. Rosenke K, Jarvis MA, Feldmann F, Schwarz B, Okumura A, Lovaglio J, et al. Hydroxychloroquine prophylaxis and treatment is ineffective in macaque and hamster SARS-CoV-2 disease models. *JCI Insight.* 2020;5(23):e143174.

13. Hansen F, Feldmann H, and Jarvis MA. Targeting Ebola virus replication through pharmaceutical intervention. *Expert Opin Investig Drugs.* 2021;30(3):201-26.

14. Rosenke K, Meade-White K, Letko M, Clancy C, Hansen F, Liu Y, et al. Defining the Syrian hamster as a highly susceptible preclinical model for SARS-CoV-2 infection. *Emerg Microbes Infect.* 2020;9(1):2673-84.

15. Corman VM, Landt O, Kaiser M, Molenkamp R, Meijer A, Chu DK, et al. Detection of 2019 novel coronavirus (2019-nCoV) by real-time RT-PCR. *Euro Surveill.* 2020;25(3):2000045.

16. Hui KPY, Ho JCW, Cheung MC, Ng KC, Ching RHH, Lai KL, et al. SARS-CoV-2 Omicron variant replication in human bronchus and lung ex vivo. *Nature.* 2022;603(7902):714-720.

17. Suzuki R, Yamasoba D, Kimura I, Wang L, Kishimoto M, Ito J, et al. Attenuated fusogenicity and pathogenicity of SARS-CoV-2 Omicron variant. *Nature.* 2022;603(7902):700-5.

18. WHO. Tracking SARS-CoV-2 variants. https://www.who.int/en/activities/tracking-SARS-CoV-2-variants/ [Accessed 11Apr22].
19. Bansal K, and Kumar S. Mutational cascade of SARS-CoV-2 leading to evolution and emergence of omicron variant. *Virus Res.* 2022;315:198765.
20. Urakova N, Kuznetsova V, Crossman DK, Sokratian A, Guthrie DB, Kolykhalov AA, et al. Beta-d-N (4)-Hydroxycytidine Is a Potent Anti-alphavirus Compound That Induces a High Level of Mutations in the Viral Genome. *J Virol.* 2018;92(3):e01965-17.
21. Toots M, Yoon JJ, Cox RM, Hart M, Sticher ZM, Makhsous N, et al. Characterization of orally efficacious influenza drug with high resistance barrier in ferrets and human airway epithelia. *Sci Transl Med.* 2019;11(515):eaax5866.
22. Agostini ML, Pruijssers AJ, Chappell JD, Gribble J, Lu X, Andres EL, et al. Small-Molecule Antiviral beta-d-N (4)-Hydroxycytidine Inhibits a Proofreading-Intact Coronavirus with a High Genetic Barrier to Resistance. *J Virol.* 2019;93(24):e01348-19.
23. Jarvis MA, Hansen FA, Rosenke K, Haddock E, Rollinson C, Rule S, et al. Evaluation of drugs for potential repurposing against COVID-19 using a tier-based scoring system. *Antivir Ther.* 2020;25(4):223-31.
24. Sia SF, Yan LM, Chin AWH, Fung K, Choy KT, Wong AYL, et al. Pathogenesis and transmission of SARS-CoV-2 in golden hamsters. *Nature.* 2020;583(7818):834-8.
25. Imai M, Iwatsuki-Horimoto K, Hatta M, Loeber S, Halfmann PJ, Nakajima N, et al. Syrian hamsters as a small animal model for SARS-CoV-2 infection and countermeasure development. *Proc Natl Acad Sci U S A.* 2020;117(28):16587-95.
26. Munoz-Fontela C, Dowling WE, Funnell SGP, Gsell PS, Riveros-Balta AX, Albrecht RA, et al. Animal models for COVID-19. *Nature.* 2020;586(7830):509-15.

27. Trimpert J, Vladimirova D, Dietert K, Abdelgawad A, Kunec D, Dokel S, et al. The Roborovski Dwarf Hamster Is A Highly Susceptible Model for a Rapid and Fatal Course of SARS-CoV-2 Infection. *Cell Rep.* 2020;33(10):108488.

28. Mehta OP, Bhandari P, Raut A, Kacimi SEO, and Huy NT. Coronavirus Disease (COVID-19): Comprehensive Review of Clinical Presentation. *Front Public Health.* 2020;8:582932.

29. Lieber CM, Cox RM, Sourimant J, Wolf JD, Juergens K, Phung Q, et al. SARS-CoV-2 variant of concern type and biological sex affect efficacy of molnupiravir in dwarf hamster model of severe COVID-19. *bioRxiv.* 2022.

30. Port JR, Yinda CK, Owusu IO, Holbrook M, Fischer R, Bushmaker T, et al. SARS-CoV-2 disease severity and transmission efficiency is increased for airborne compared to fomite exposure in Syrian hamsters. *Nat Commun.* 2021;12(1):4985.

FIGURES

Figure 1

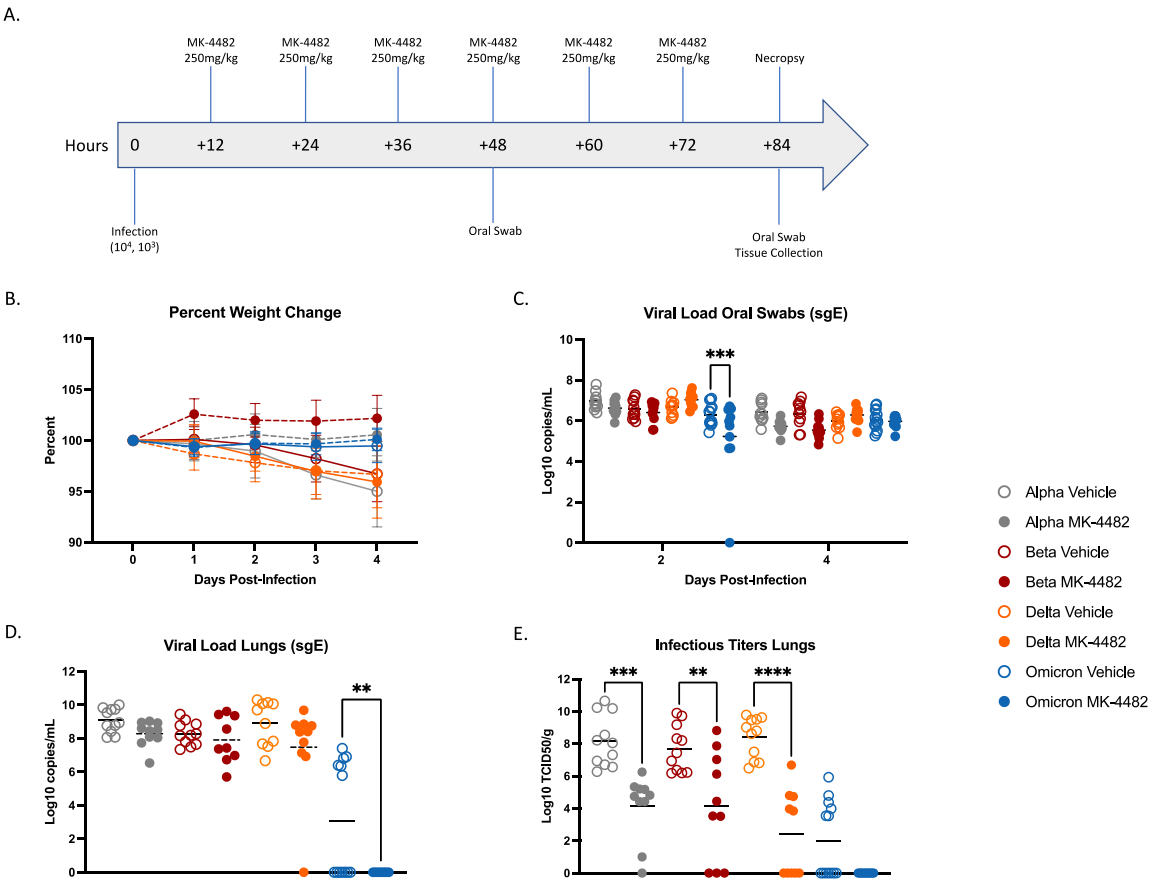

Figure 1. MK-4482 efficacy on upper and lower respiratory tract viral load and infectivity in hamsters infected with SARS-CoV-2 Alpha, Beta, Delta and Omicron VOCs. (A) Experimental design. Hamsters (N =11 vehicle, 10 treatment) were intranasally infected with

10^3 $TCID_{50}$ of the different SARS-CoV-2 VOCs. Treatment was started 12 hours post infection and continued every 12 hours. Oral swabs were collected on 2 and 4 dpi and animals were necropsied on 4 dpi for tissue collection. **(B) Clinical presentation.** Changes in body weight were recorded over the entire study period of 4 days. **(C) Viral RNA load in oral swabs.** Alpha, Beta, Delta and Omicron RNA loads were determined by quantitative RT-PCR targeting sgE RNA as a surrogate for replication and shedding. **(D) Viral RNA loads in lung tissue.** Alpha, Beta, Delta and Omicron RNA loads were determined by quantitative RT-PCR targeting sgE as a surrogate for replication. **(E) Infectious viral titers in lung tissue.** Alpha, Beta, Delta and Omicron infectivity was determined using a tissue culture infectious dose (TCID) assay and are presented as $TCID_{50}$/gram tissue. Statistical differences in viral load and infectious virus titers in each study arm were assessed by ordinary one-way ANOVA ($p<0.05$).

Figure 2

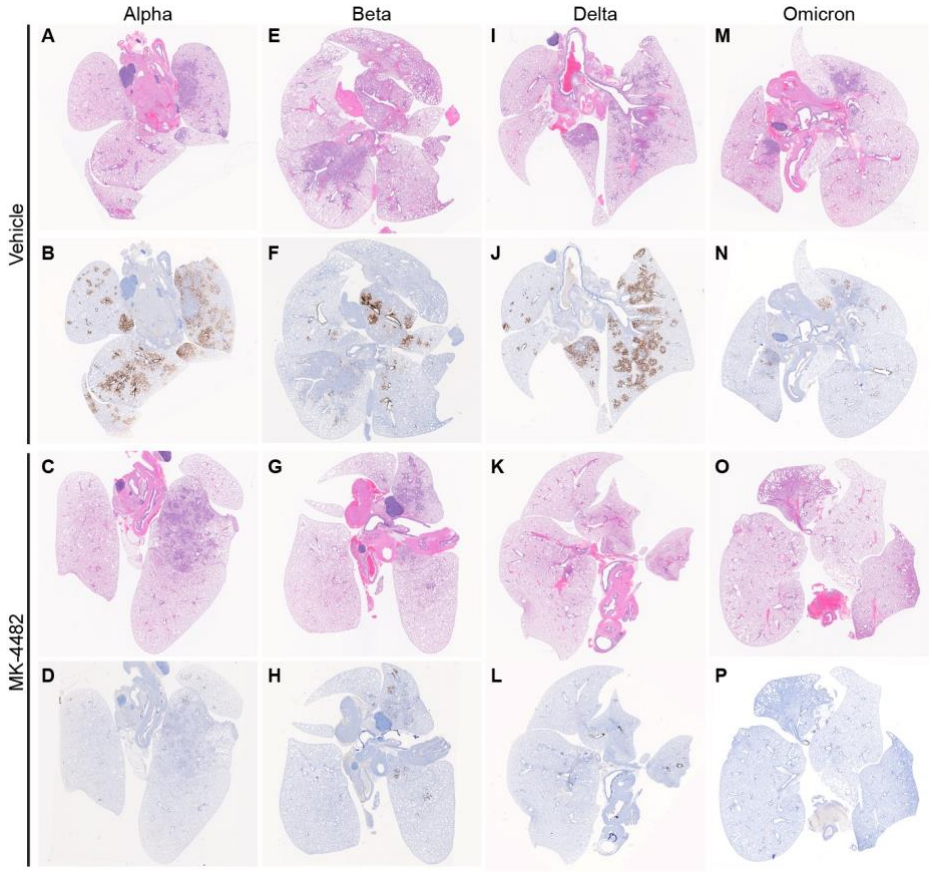

Figure 2: MK-4482 efficacy on lung tissue from SARS-CoV-2 Alpha, Beta, Delta and Omicron VOC infected hamsters. The experimental design is shown in Figure 1A. Lung tissue was collected on 4 dpi and prepared for hematoxylin and eosin (H&E) stain and immunohistochemistry (IHC) using an antibody directed against the SARS-CoV-2 nucleocapsid protein. (**A, E, I, M**.) **Lung histopathology.** H&E stain of lung tissue from vehicle treated hamsters infected with Alpha, Beta, Delta and Omicron VOC, respectively. Areas of consolidation represent foci of broncho-interstitial pneumonia. (**B, F, J, N**) **Lung immunohistochemistry.** SARS-CoV-2 nucleoprotein detection in lung section from vehicle-treated hamsters infected with Alpha, Beta, Delta and Omicron, respectively. Corresponding foci of immunoreactivity (brown color) are shown. (**C, G, K, O**) **Lung histopathology.** H&E

stain of lung tissue from MK-4482 treated hamsters infected with Alpha, Beta, Delta and Omicron VOC, respectively. Areas of consolidation represent foci of broncho-interstitial pneumonia. (**D, H, L, P) Lung immunohistochemistry.** SARS-CoV-2 nucleoprotein detection in lung section from MK-4482 treated hamsters infected with Alpha, Beta, Delta and Omicron, respectively. Corresponding foci of immunoreactivity (brown color) are shown. Whole lung sections are shown.

Figure 3

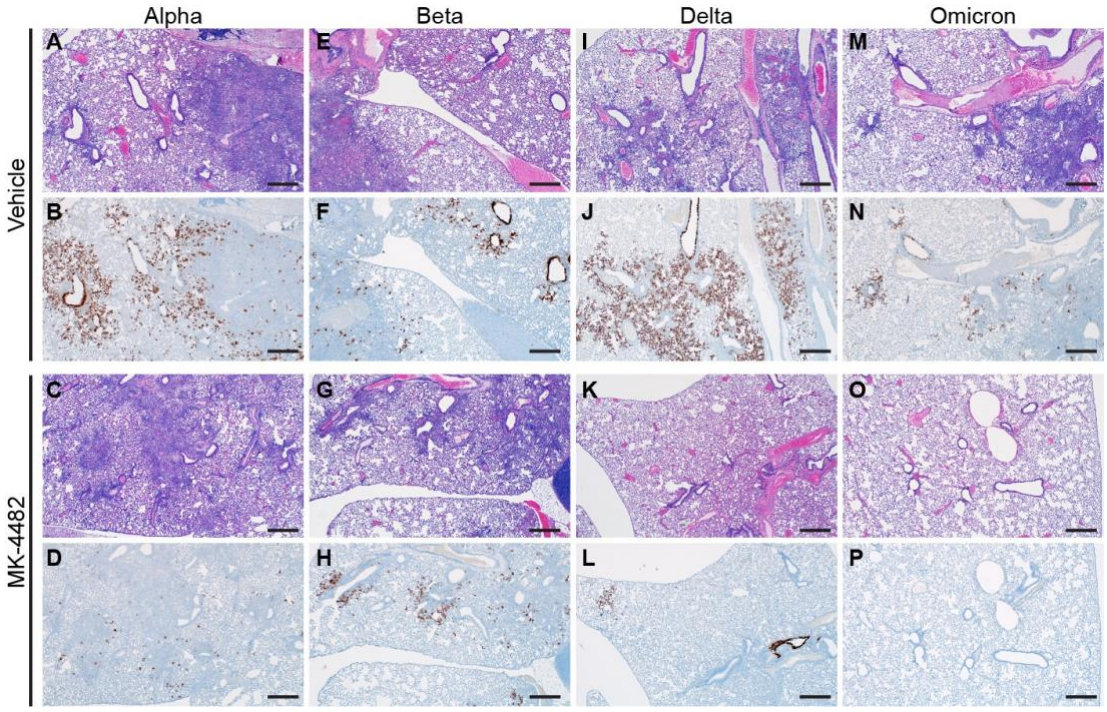

Figure 3: MK-4482 efficacy on lung pathology in hamsters infected with multiple SARS-CoV-2 VOCs. The experimental design is shown in Figure 1A. Lung tissue was collected on 4 dpi and prepared for H&E stain and IHC using an antibody directed against the SARS-CoV-2 nucleocapsid protein. **(A, E, I, M) Lung H&E (40x).** H&E stains from vehicle treated hamsters infected with Alpha, Beta, Delta and Omicron VOC, respectively, showing bronchointerstitial pneumonia and vasculitis. **(B, F, J, N) Lung IHC (40x).** SARS-CoV-2 nucleoprotein detection in lung section from vehicle-treated hamsters infected with Alpha, Beta, Delta and Omicron, respectively, exhibiting immunoreactivity associated with areas of pneumonia (brown color). **(C, G, K, O) Lung H&E (40x).** H&E stain from MK-4482 treated hamsters infected with Alpha, Beta, Delta and Omicron VOC, respectively, showing reduced bronchointerstitial pneumonia.

(D, H, L, P) Lung IHC (40x). SARS-CoV-2 nucleoprotein detection in lung section from MK-4482 treated hamsters infected with Alpha, Beta, Delta and Omicron VOC, respectively, exhibiting reduced or no immunoreactivity. Each panel shows a lung section from a representative hamster. Bar = 500μm

Figure 4

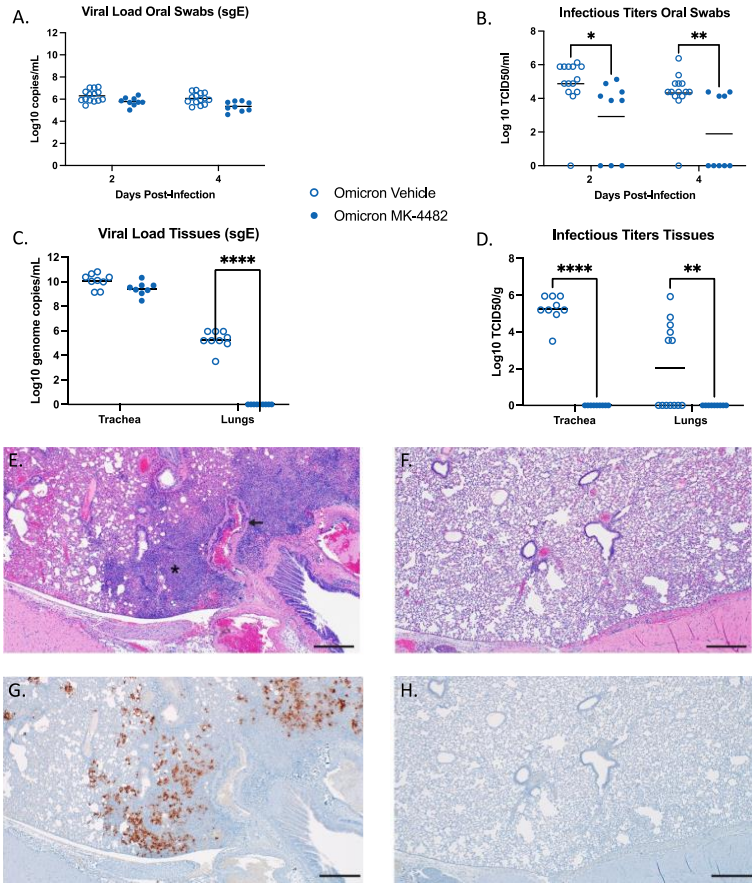

Figure 4. MK-4482 efficacy on upper and lower respiratory tract viral load, infectivity and lung pathology in hamsters infected with high dose Omicron SARS-CoV-2 VOC. The experimental design is shown in Figure 1A. For this experiment we used an Omicron challenge dose of 10^4 $TCID_{50}$ and collected trachea as an additional tissue. **(A) Omicron RNA load in oral swabs.** Viral loads were determined by quantitative RT-PCR targeting sgE RNA as a surrogate for replication and shedding. **(B) Infectious Omicron titers in oral swabs.** Viral infectivity was determined using a $TCID_{50}$ assay and are presented as $TCID_{50}$/gram tissue. **(C) Omicron loads in trachea and lung tissues.** Viral loads were determined by quantitative RT-PCR targeting sgE RNA as a surrogate for replication. **(D) Infectious Omicron titers in trachea and lung tissues.** Viral infectivity was determined using a $TCID_{50}$ assay and are presented as

$TCID_{50}$/gram tissue. Statistical analysis was performed in Prism 9. **(E) Lung H&E (40x).** Lung H&E of a vehicle treated hamster infected with Omicron exhibiting a focus of bronchointerstitial pneumonia (asterisk) and vasculitis (arrow). **(F) Lung H&E (40x).** Lung H&E of a MK-4482 treated hamster infected with Omicron showing normal pathology. **(G) Lung IHC (40x).** Lung IHC from a vehicle treated hamster infected with Omicron exhibiting frequent immunoreactivity associated with focus of pneumonia (brown color). **(H) Lung IHC (40x).** Lung IHC of a MK-4482 treated hamster infected with Omicron exhibiting absence of immunoreactivity. Each panel shows a lung section from a representative hamster. Bar = 500 μm. Statistical differences in viral load and infectious virus titers in each study arm were assessed by ordinary one-way ANOVA ($p<0.05$).

.